Chemical Reaction Monitoring using Zero-Field Nuclear Magnetic Resonance Enables Study of Heterogeneous Samples in Metal Containers**

Dudari B. Burueva[+], James Eills[+], John W. Blanchard,* Antoine Garcon, Román Picazo-Frutos, Kirill V. Kovtunov, Igor V. Koptyug, and Dmitry Budker*

Abstract: We demonstrate that heterogeneous/biphasic chemical reactions can be monitored with high spectroscopic resolution using zero-field nuclear magnetic resonance spectroscopy. This is possible because magnetic susceptibility broadening is negligible at ultralow magnetic fields. We show the two-step hydrogenation of dimethyl acetylenedicarboxylate with para-enriched hydrogen gas in conventional glass NMR tubes, as well as in a titanium tube. The low frequency zero-field NMR signals ensure that there is no significant signal attenuation arising from shielding by the electrically conductive sample container. This method paves the way for in situ monitoring of reactions in complex heterogeneous multiphase systems and in reactors made of conductive materials while maintaining resolution and chemical specificity.

Introduction

High-field nuclear magnetic resonance (HF NMR) spectroscopy is a powerful analytical tool for reaction monitoring, as it provides structural and chemical information about a sample in a quantitative and non-invasive manner. However, the operation of conventional NMR spectrometers imposes substantial restrictions on its applicability for in situ reaction monitoring. Reactions carried out in metallic containers cannot be addressed by HF NMR (typically, NMR sample containers are made of glass, quartz, plastic or ceramic), and heterogeneous samples generally yield low-resolution spectra owing to magnetic susceptibility induced

field gradients.[1,2] Nevertheless, NMR spectroscopy is extensively applied for analyses of reactions conducted in NMR tubes,[3,4] and for offline analysis of aliquots from chemical reactors.[5] More advanced approaches such as rapid injection[6–8] and stopped-flow analysis[9–11] have been proposed to study rapid kinetics and have allowed direct observation of reactive intermediate species. However, these approaches are not generally compatible with operando analyses.[12] To overcome this drawback online NMR reaction monitoring was introduced, which involves transfer of a homogeneous reaction mixture from a reactor to the NMR magnet for the detection of the flowing sample without the need for discrete sampling or exposing the reaction mixture to the external atmosphere.[13–19] At the same time, the studies of heterogeneous reactors and reacting systems[20,21] require different experimental approaches.

An alternative approach is to use zero- to ultralow-field (ZULF) NMR,[22–26] in which the NMR experiment is performed in the absence of a strong[°] external magnetic field. This is the regime in which, in contrast to HF NMR, intramolecular J-couplings (electron-mediated indirect nuclear spin–spin couplings) are the dominant interaction, and the nuclear Zeeman interaction may be treated as a perturbation.[27] By operating under these conditions, there is negligible magnetic susceptibility broadening for heterogeneous samples (e.g. in biphasic or porous media),[26] and the low-frequency magnetic fields readily penetrate metals.[28] As an example, the depth of penetration of an oscillating magnetic field (the skin

[*] D. B. Burueva,[+] Dr. K. V. Kovtunov, Prof. I. V. Koptyug
Laboratory of Magnetic Resonance Microimaging, International
Tomography Center
630090 Novosibirsk (Russia)
and
Novosibirsk State University
630090 Novosibirsk (Russia)

Dr. J. Eills,[+] Dr. J. W. Blanchard, A. Garcon, R. Picazo-Frutos,
Prof. D. Budker
Helmholtz Institute Mainz
GSI Helmholtzzentrum für Schwerionenforschung GmbH
55128 Mainz (Germany)
E-mail: eills@uni-mainz.de
          blanchard@uni-mainz.de

Dr. J. Eills,[+] A. Garcon, R. Picazo-Frutos, Prof. D. Budker
Johannes Gutenberg University
55090 Mainz (Germany)

Prof. D. Budker
University of California Berkeley
Berkeley, CA 94720 (USA)

[+] These authors contributed equally to this work.

[°] "Strong" corresponds to the condition $|\gamma_1 B - \gamma_2 B| \gg 2\pi |J_{12}|$, with γ_i the gyromagnetic ratio of spin i, B the magnetic field strength, and J_{ij} the J coupling between spins i and j.

depth) for stainless steel at a frequency of 100 MHz is approximately 42 mm, but increases to around 42 mm at 100 Hz. Moreover, in ZULF NMR, narrow resonance linewidths can be achieved, allowing for precise measurements of J-couplings.[29] Since J-couplings are dependent on molecular structure, this allows for chemical fingerprinting and analysis[30,31] despite the fact that chemical shift information is not available at these magnetic fields. The combination of narrow linewidths due to the absence of susceptibility broadening and the ability to measure inside metal containers makes ZULF NMR a promising technique for in situ chemical reaction monitoring under practical conditions.

In HF NMR, nuclear spins are typically polarized prior to detection by the large magnetic field of an NMR instrument. In ZULF NMR, several alternative sample polarization modalities have been demonstrated, including sample pre-polarization in an external field,[26] and sample hyperpolarization.[32–36] Parahydrogen-induced polarization (PHIP)[37,38] is a class of hyperpolarization techniques which deliver spin polarization to a sample by way of a nuclear spin isomer of the hydrogen molecule, namely parahydrogen, characterized by zero total nuclear spin of the two hydrogen atoms. Para-enriched hydrogen (p-H_2) can be generated by cooling hydrogen gas in the presence of a paramagnetic material.[39] In PHIP, the singlet spin order of parahydrogen can be converted into enhanced (nonequilibrium) nuclear magnetization of the hydrogenation product if p-H_2 is added in a pairwise manner to an unsaturated precursor using a suitable hydrogenation catalyst.[40] Spin-polarization levels of a few to a few tens of % can be achieved with PHIP depending on experimental implementation.[41–48] In ZULF NMR experiments, enhanced signals can be observed if there is a hetero-nuclear spin present in the molecule which renders the parahydrogen-derived protons magnetically inequivalent.[32]

In this work we study two-step hydrogenation of an unsaturated precursor molecule with para-enriched hydrogen gas using ZULF NMR. This is done by continuously bubbling the hydrogen gas into samples containing dissolved dimethyl acetylenedicarboxylate (DMAD) along with the appropriate catalyst, and observing the NMR signals of the hydrogenation products (dimethyl maleate and dimethyl succinate) over time with a commercial atomic magnetometer.[49] Magnetic shielding and compensating coils are used to create the "zero-field" region, with residual magnetic-field intensity on the order of 10–100 pT, although the magnetometer can operate in fields up to 50 nT. A schematic of the experimental setup is shown in Figure 1.

Results and Discussion

In all experiments, the initial reaction solution was 500 mM DMAD and 5 mM [Rh(dppb)(COD)]BF_4 catalyst in [D_6]acetone. Deuterated acetone was used to extend the lifetime of hyperpolarized spin order. Figure 2 shows a ZULF NMR spectrum acquired while bubbling para-enriched hydrogen gas into 2 mL of reaction solution in a titanium NMR tube. The spectrum is the average of 32 transients. Experimental details can be found in the
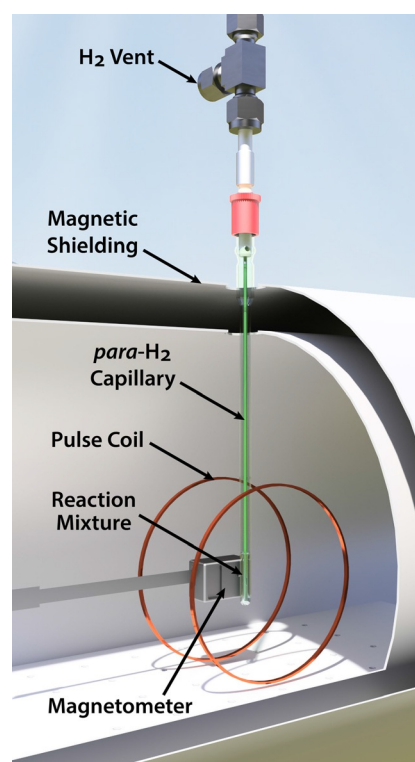

Figure 1. Schematic of the experimental setup. An NMR tube (5 mm outside diameter (O.D.) glass, or 12 mm O.D. titanium) containing the sample is held in the center of a magnetically shielded volume. An atomic magnetometer is positioned adjacent to the sample, and a Helmholtz coil pair is used to apply magnetic-field pulses along the sensitive axis of the magnetometer. Further details are provided in the Materials and Methods section of the Supporting Information.

Materials and Methods section of the Supporting Information.

One set of peaks at 160–172 Hz corresponds to $^1J_{CH}$ ≈ 167 Hz, the one-bond coupling of a parahydrogen-derived proton to the ^{13}C nucleus (at 2.2 % natural abundance due to the molecular symmetry) in dimethyl maleate, split by coupling to the proton of its second methine (^{12}CH) group. A second set of peaks at 185–205 Hz corresponds to 3/2 × 133 Hz one-bond ^1H–^{13}C coupling in dimethyl succinate, split by coupling to the protons in the other methylene ($^{12}CH_2$) group. A simulated spectrum is shown beneath, and details of the simulations can be found in the Supporting Information. There is an additional peak in the succinate spectrum at 195 Hz that is not accounted for in the simulation, even if a term in the initial density matrix corresponding to hyper-polarized spin order carried over from maleate is included. This peak grows and shrinks at the same rate as the other succinate peaks over the course of the reaction and is possibly a side product such as monomethyl succinate or succinic anhydride; this is subject to further investigation.

The J-couplings in the two product molecules are shown in Figure 3. Some J-coupling values were taken from the literature[50] as a starting point, and then the couplings were adjusted until the simulated spectra fit the data. We are able to extract not only the magnitude of the J-couplings, but also the relative signs. In addition, the zero-field spectra reveal
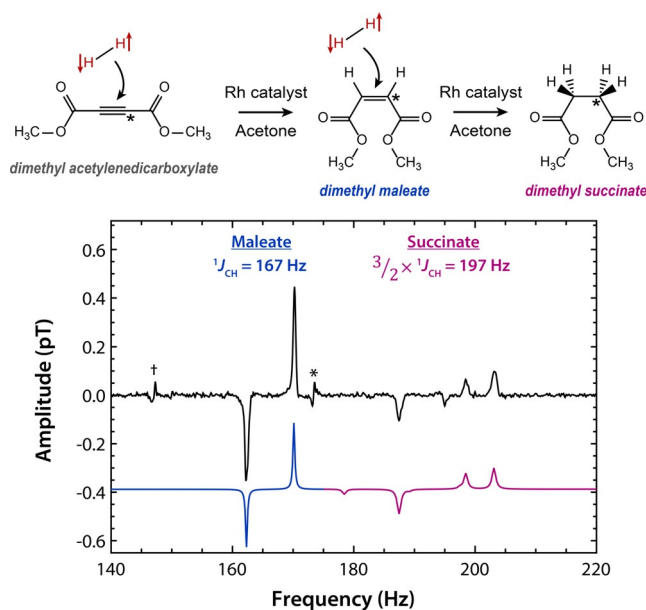
Figure 2. Top: the chemical reaction under investigation. DMAD is doubly hydrogenated in the reaction. Natural isotopic abundance DMAD is used (2.2% ^{13}C nuclei in the position indicated by the asterisk and its symmetric counterpart). ^{13}C in other positions gives peaks at frequencies outside the displayed window. Bottom: a representative spectrum (black) acquired with 32 transients during the chemical reaction in a titanium tube. A simulated spectrum is shown beneath. The $^{1}J_{CH}$ coupling dominates in each molecule, producing groups of peaks around 167 Hz (J) for the CH group of maleate, and approximately 200 Hz ($3J/2$) for the CH$_2$ group in succinate. There are noise peaks at $50n$ Hz ($n=0,1,2...$) from the line noise and its overtones, as well as at $100n \pm 27$ Hz (marked with an asterisk), which arise from the QuSpin's 923 Hz internal modulation mixing with the line noise. There is also a peak at 147.3 Hz (and 294.6 Hz) marked with a dagger, which comes from the molecules in which there is a ^{13}C spin in one or both of the methyl groups; this is discussed further in the Supporting Information.
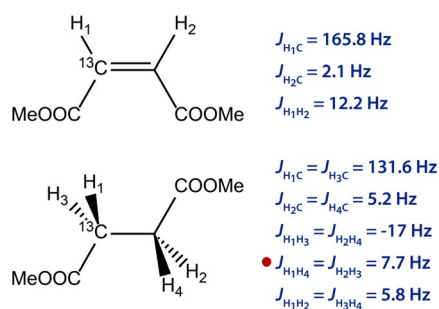

Figure 3. The dimethyl maleate and dimethyl succinate J-couplings used to generate the simulated spectra in Figure 2. Couplings to the methyl protons were not included in simulations. The red dot indicates which proton pair in dimethyl succinate is thought to originate from parahydrogen.

details about the stereochemistry of the catalytic products. It has been reported in the literature that J_{H1H4} is larger than J_{H1H2},[50] and from this we were able to determine that the second p-H$_2$ proton pair likely occupies positions H$_1$ + H$_4$ (or equivalently H$_2$ + H$_3$) on the final product. Details on how the

simulations were performed are given in the Supporting Information.

The hydrogenation reaction was then monitored in a pressurizable 5 mm glass NMR tube at three different hydrogen pressures by acquiring a spectrum every 5 s while continuously bubbling *para*-enriched hydrogen gas into a 400 µl reaction solution at 50 mL min^{-1}. The time dependences of the dimethyl maleate and dimethyl succinate peak integrals are plotted in Figure 4, and show signal build-up and decay for both reaction products. The peak widths are expected to give a precise measure of the relaxation time of the observable coherences (T_2) since there is no additional line broadening from magnetic susceptibility inhomogeneity. The relaxation times were measured to be 0.7 s for maleate, and 0.5 s for succinate. Since we observe the molecules in
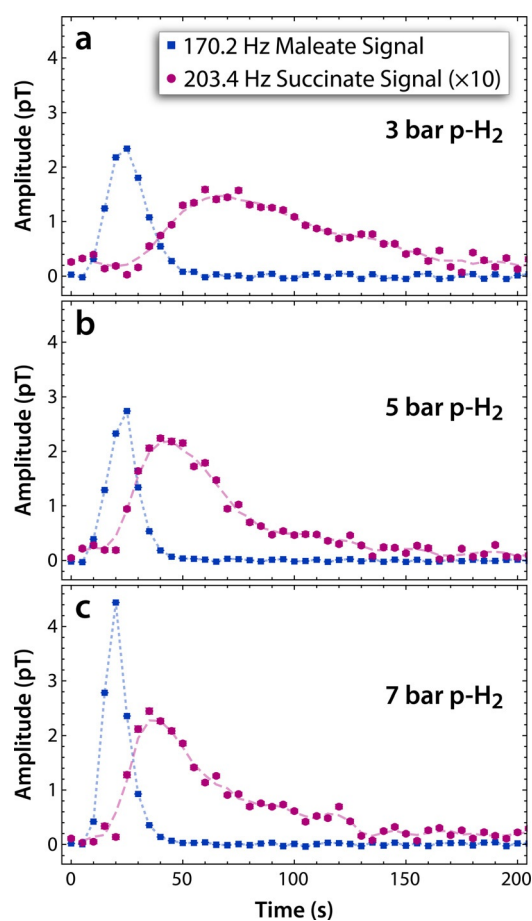

Figure 4. The time-dependence of the maleate (blue squares) and succinate (magenta circles) NMR signals is shown for reactions carried out at three p-H$_2$ pressures. Signals were acquired during continuous p-H$_2$ bubbling, and each data point was generated by integrating the indicated signal. See the Materials and Methods section of the Supporting Information for further details. The succinate peak integrals are lower than those for maleate because hyperpolarized succinate is in lower concentration in each scan, and there are more lines in the J-spectra but only one is integrated. Error bars are the standard error on the peak fitting, but are mostly contained within the plot markers. Note that since each pulse converts all available spin order into observable coherences, the signal observed in each scan represents the concentration of product formed since the previous scan, rather than total concentration of product molecules.

which a proton is directly bound to a ^{13}C, the proximity of the spins in space suggests the relatively rapid relaxation is likely dominated by the fluctuating intra-pair dipole–dipole coupling. We have not measured the relaxation time constant of populations in this system (T_1). The maleate signals additionally decay as the species is further hydrogenated into succinate. It should be noted that the application of the magnetic field pulse to observe the reaction products destroys the signals, and so neglecting relaxation effects, the signal seen in each scan corresponds only to the product formed after the previous pulse.

The experiment was then repeated for a 2 mL sample in a titanium tube (12 mm outer diameter, 10 mm inner diameter), using parahydrogen pressurized at 5 bar. The peak integrals are plotted in Figure 5, alongside a schematic showing the metal tube. The product peaks are visible for a longer duration because a larger sample volume was used, but the p-H_2 flow rate was the same.
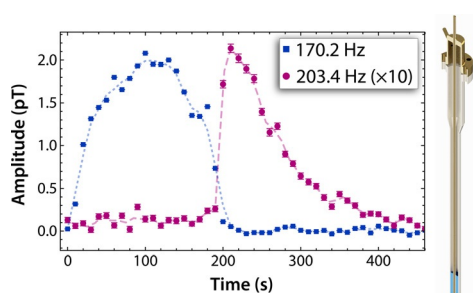

Figure 5. The time-dependence of the maleate (blue squares) and succinate (magenta circles) NMR signals, for a reaction carried out at 5 bar p-H_2 pressure in a titanium tube (shown to the right). Signals were acquired during continuous bubbling. The signals persist for longer than in Figure 4b because the sample volume here was larger by a factor of five. The signals observed here are marginally lower in amplitude than those shown in Figure 4b due to the difference in distance between the magnetometer and sample. See the Materials and Methods section of the Supporting Information for details.

Hydrogenation of DMAD over cationic Rh catalysts is known to proceed via *syn*-addition of two hydrogen atoms to the carbon-carbon triple bond, giving predominantly dimethyl maleate, the *cis*-conformer of the product molecule. The latter possesses a carbon-carbon double bond and can be hydrogenated further to dimethyl succinate. Both the spectra (Figure 2) and the kinetics (Figure 4, Figure 5), are in agreement with this reaction mechanism.[51,52] At the same time, it should be noted that for hyperpolarized molecules the nuclear spin relaxation processes mentioned above significantly affect the integrated NMR signal intensities which, as a result, are not proportional to respective concentrations. Therefore, a quantitative analysis of the kinetic traces presented in Figure 4, Figure 5 is not trivial, and is beyond the scope of this study. Nevertheless, some useful information on this reacting system can be obtained even from a qualitative data analysis.

Firstly, it is seen that the reaction timescale depends measurably on the availability of H_2 in the system—at higher pressures it takes less time for the reaction to complete

(Figure 4), whereas increasing the reaction volume at the same pressure and flow rate of H_2 slows the reaction down (Figure 5 vs. Figure 4b). These observations are in accord with the accepted reaction mechanism for hydrogenation over cationic rhodium complexes, in which coordination of the unsaturated substrate to the complex takes place first, followed by the oxidative addition of H_2 in the rate-determining step.[53–56] Higher H_2 pressures and smaller sample volumes lead to higher concentrations of dissolved H_2 and accelerate the reaction.

Secondly, it is known that alkynes coordinate to metal complexes more strongly than alkenes, which has two opposing consequences for hydrogenation. For most catalysts, stronger binding of the alkyne results in a lower intrinsic rate of hydrogenation compared to that for the corresponding alkenes.[53,57] However, when both are present in the reaction system, stronger binding of alkyne allows it to outcompete the alkene in binding to the catalyst, which can result in high selectivities toward alkene production in selective alkyne hydrogenation even at high alkyne conversions.[52,58] This type of behavior can be seen in Figure 5. Remarkably, almost no dimethyl succinate formation is observed within around the first 200 s of the reaction; during this time interval the NMR spectra are dominated by the signals of hyperpolarized dimethyl maleate. Only after about 200 s of reaction, the signals of dimethyl succinate start to increase sharply, signifying the moment when DMAD is essentially consumed and competition for the active center is over.

A number of experimental parameters determine how efficient the competition for the metal center between alkyne and alkene is, including hydrogen pressure and the alkyne/catalyst ratio.[59] In particular, for higher H_2 pressures the hydrogenation events proceed faster (cf. Figure 4), implying that the dimethyl maleate molecule which was just formed on the catalytic center and still remains bound to the catalyst has a larger probability to be hydrogenated further to dimethyl succinate before it is kicked out from the catalyst by a DMAD molecule. The onset of dimethyl succinate formation quite early in the DMAD hydrogenation reaction was observed, for instance, in a recent NMR study which used DMAD hyperpolarized by dissolution DNP.[60] The DMAD/catalyst ratio in that study was around 5-fold lower compared to our work, and besides the catalyst was undergoing activation during the measurements.

Next we compare the spectra detected while continually bubbling parahydrogen gas during signal acquisition to the ones in which gas flow was stopped before signal acquisition was started. This comparison clearly shows that in high-field NMR (Figure 6a) the sample heterogeneity induced by bubbling gas through the sample reduces the spectral resolution dramatically compared to homogeneous samples. We repeated these experiments at zero-field, with the heterogeneous-sample experiment performed in the titanium tube using 10 bar of parahydrogen gas. The results shown in Figure 6b clearly demonstrate that in ZULF NMR the spectral resolution is largely immune to heterogeneities produced by gas bubbling during signal acquisition.

Using a titanium tube allowed for reactions to be carried out at higher pressure than was possible with the glass tubes.
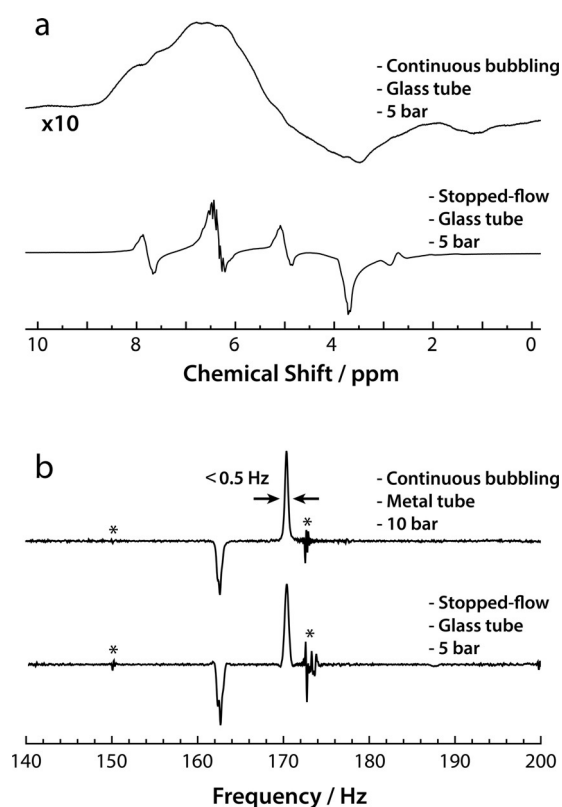
Figure 6. Representative spectra showing that high-field NMR spectroscopy (a) suffers from low resolution for heterogeneous samples (i.e. caused by bubbling a gas) as a result of magnetic susceptibility broadening, but this is not the case for zero-field NMR spectroscopy (b) under similar conditions. Additionally, there is no detectable line broadening and signal loss from the use of a titanium tube instead of a 5 mm glass NMR tube. The rate of bubbling used in all experiments was 50 mL min⁻¹, and "stopped-flow" means the bubbling was stopped prior to signal acquisition. Asterisks denote noise peaks in the ZULF spectra.

As mentioned in the Introduction, this is possible using ZULF NMR due to the larger skin depth for conductive metals at lower frequencies. Titanium was chosen as a nonmagnetic metal, but we anticipate that other metals may be appropriate (perhaps after degaussing). Considering that industrial reactors are typically operated at high temperatures and pressures that are only practically attainable in metal containers, ZULF NMR is uniquely capable of non-invasive reaction monitoring under realistic conditions. Metal reactors would be indispensable for studying such industrially important reactions as synthesis of liquid hydrocarbons from H_2/CO synthesis gas in the Fischer–Tropsch process (pressures of several tens of bar), or production of ammonia from N_2 and H_2 in the Haber-Bosch process (several hundred bar).

In high-field NMR, nuclear spins are polarized by the large magnetic field; in zero-field NMR of bulk samples, an external source of nuclear spin polarization is required. We used chemical reaction with para-enriched hydrogen gas for this demonstration; a number of alternative approaches have been shown in the context of ZULF NMR.[36,61] A closely related analogue to hydrogenative PHIP (including its heterogeneous version[62]) is signal amplification by reversible

exchange (SABRE),[63–65] in which the hyperpolarized spin order of para-enriched hydrogen is transferred to other molecules via reversible exchange on a suitable metal-containing catalyst. Another option is to pre-polarize the molecules in an external magnetic field prior to detection. The field of hyperpolarized NMR is growing rapidly, and yet more polarization techniques are being explored for application to ZULF NMR.

Conclusion

In conclusion, we have demonstrated zero-field NMR spectroscopy as a method for reaction monitoring with chemical specificity by detecting the hydrogenation of molecules with para-enriched hydrogen gas. We were able to extract *J*-couplings and their relative signs from the zero-field spectra. For these experiments a commercial atomic magnetometer was used for signal detection. The advantages of this analytical technique are the ability to observe samples in metal containers, and to maintain spectral resolution in samples exhibiting inhomogeneous magnetic susceptibility. We expect that if the spin relaxation times are measured, quantitative kinetic parameters can be extracted using this technique. We anticipate that ZULF NMR will find application in the field of catalysis for operando and in situ reaction monitoring, as well as the study of chemical reaction mechanisms under realistic conditions. We are exploring the possibility of implementing an array of magnetic sensors around a reactor for spatially resolved chemical kinetics monitoring.

Acknowledgements

Conflict of interest

The authors declare no conflict of interest.

[1] M. E. Stoll, T. J. Majors, *J. Magn. Reson.* **1982**, *46*, 283–288.

[2] A. I. Svyatova, K. V. Kovtunov, I. V. Koptyug, *Rev. Chem. Eng.* **2019**, https://doi.org/10.1515/revce-2018-0035

[3] M. H. M. Killner, Y. Garro Linck, E. Danieli, J. J. R. Rohwedder, B. Blümich, *Fuel* **2015**, *139*, 240–247.

[4] A. Friebel, E. von Harbou, K. Münnemann, H. Hasse, *Ind. Eng. Chem. Res.* **2019**, *58*, 18125–18133.

[5] A. Friebel, E. von Harbou, K. Münnemann, H. Hasse, *Chem. Eng. Sci.* **2020**, *219*, 115561.

[6] A. C. Jones, A. W. Sanders, W. H. Sikorski, K. L. Jansen, H. J. Reich, *J. Am. Chem. Soc.* **2008**, *130*, 6060–6061.

[7] S. E. Denmark, B. J. Williams, B. M. Eklov, S. M. Pham, G. L. Beutner, *J. Org. Chem.* **2010**, *75*, 5558–5572.

[8] A. C. Jones, A. W. Sanders, M. J. Bevan, H. J. Reich, *J. Am. Chem. Soc.* **2007**, *129*, 3492–3493.

[9] M. D. Christianson, E. H. P. Tan, C. R. Landis, *J. Am. Chem. Soc.* **2010**, *132*, 11461–11463.

[10] C. P. Johnston, T. H. West, R. E. Dooley, M. Reid, A. B. Jones, E. J. King, A. G. Leach, G. C. Lloyd-Jones, *J. Am. Chem. Soc.* **2018**, *140*, 11112–11124.

[11] A. L. Dunn, C. R. Landis, *Magn. Reson. Chem.* **2017**, *55*, 329–336.

[12] D. A. Foley, M. T. Zell, A. L. Dunn, *Magn. Reson. Chem.* **2016**, *54*, 451–456.

[13] S. S. Zalesskiy, E. Danieli, B. Blümich, V. P. Ananikov, *Chem. Rev.* **2014**, *114*, 5641–5694.

[14] V. Sans, L. Porwol, V. Dragone, L. Cronin, *Chem. Sci.* **2015**, *6*, 1258–1264.

[15] P. Giraudeau, F.-X. Felpin, *React. Chem. Eng.* **2018**, *3*, 399–413.

[16] J. Eills, W. Hale, M. Sharma, M. Rossetto, M. H. Levitt, M. Utz, *J. Am. Chem. Soc.* **2019**, *141*, 9955–9963.

[17] D. Kreyenschulte, E. Paciok, L. Regestein, B. Blümich, J. Büchs, *Biotechnol. Bioeng.* **2015**, *112*, 1810–1821.

[18] M. V. Silva Elipe, R. R. Milburn, *Magn. Reson. Chem.* **2016**, *54*, 437–443.

[19] K. C. H. Tijssen, B. J. A. Weerdenburg, H. Zhang, J. W. G. Janssen, M. C. Feiters, P. J. M. Bentum, A. P. M. Kentgens, *Anal. Chem.* **2019**, *91*, 12636–12643.

[20] A. A. Lysova, I. V. Koptyug, *Chem. Soc. Rev.* **2010**, *39*, 4585–4601.

[21] J. Ulpts, W. Dreher, M. Klink, J. Thöming, *Appl. Catal. A* **2015**, *502*, 340–349.

[22] J. W. Blanchard, D. Budker, *eMagRes* **2016**, *5*, 1395–1410.

[23] M. C. D. Tayler, T. Theis, T. F. Sjolander, J. W. Blanchard, A. Kentner, S. Pustelny, A. Pines, D. Budker, *Rev. Sci. Instrum.* **2017**, *88*, 091101.

[24] M. Mößle, S. I. Han, W. R. Myers, S. K. Lee, N. Kelso, M. Hatridge, A. Pines, J. Clarke, *J. Magn. Reson.* **2006**, *179*, 146–151.

[25] M. C. D. Tayler, J. Ward-Williams, L. F. Gladden, *Appl. Phys. Lett.* **2019**, *115*, 072409.

[26] M. C. D. Tayler, J. Ward-Williams, L. F. Gladden, *J. Magn. Reson.* **2018**, *297*, 1–8.

[27] M. P. Ledbetter, T. Theis, J. W. Blanchard, H. Ring, P. Ganssle, S. Appelt, B. Blümich, A. Pines, D. Budker, *Phys. Rev. Lett.* **2011**, *107*, 107601.

[28] S. Xu, E. Harel, D. J. Michalak, C. W. Crawford, D. Budker, A. Pines, *J. Magn. Reson. Imaging* **2008**, *28*, 1299–1302.

[29] A. Wilzewski, S. Afach, J. Blanchard, D. Budker, *J. Magn. Reson.* **2017**, *284*, 66–72.

[30] R. Mcdermott, A. H. Trabesinger, M. Mück, E. L. Hahn, A. Pines, J. Clarke, *Science* **2002**, *295*, 2247–2249.

[31] J. W. Blanchard, M. P. Ledbetter, T. Theis, M. C. Butler, D. Budker, A. Pines, *J. Am. Chem. Soc.* **2013**, *135*, 3607–3612.

[32] M. C. Butler, G. Kervern, T. Theis, M. P. Ledbetter, P. J. Ganssle, J. W. Blanchard, D. Budker, A. Pines, *J. Chem. Phys.* **2013**, *138*, 234201.

[33] T. Theis, M. P. Ledbetter, G. Kervern, J. W. Blanchard, P. J. Ganssle, M. C. Butler, H. D. Shin, D. Budker, A. Pines, *J. Am. Chem. Soc.* **2012**, *134*, 3987–3990.

[34] T. Theis, M. L. Truong, A. M. Coffey, R. V. Shchepin, K. W. Waddell, F. Shi, B. M. Goodson, W. S. Warren, E. Y. Chekmenev, *J. Am. Chem. Soc.* **2015**, *137*, 1404–1407.

[35] J. Eills, J. W. Blanchard, T. Wu, C. Bengs, J. Hollenbach, D. Budker, M. H. Levitt, *J. Chem. Phys.* **2019**, *150*, 174202.

[36] H. J. Lee, S.-J. Lee, J. H. Shim, H. S. Moon, K. Kim, *J. Magn. Reson.* **2019**, *300*, 149–152.

[37] C. R. Bowers, D. P. Weitekamp, *J. Am. Chem. Soc.* **1987**, *109*, 5541–5542.

[38] R. A. Green, R. W. Adams, S. B. Duckett, R. E. Mewis, D. C. Williamson, G. G. R. Green, *Prog. Nucl. Magn. Reson. Spectrosc.* **2012**, *67*, 1–48.

[39] B. Feng, A. M. Coffey, R. D. Colon, E. Y. Chekmenev, K. W. Waddell, *J. Magn. Reson.* **2012**, *214*, 258–262.

[40] M. Emondts, J. F. P. Colell, B. Blümich, P. P. M. Schleker, *Phys. Chem. Chem. Phys.* **2017**, *19*, 21933–21937.

[41] R. V. Shchepin, D. A. Barskiy, A. M. Coffey, Manzanera, I. V. Esteve, E. Y. Chekmenev, *Angew. Chem. Int. Ed.* **2016**, *55*, 6071–6074; *Angew. Chem.* **2016**, *128*, 6175–6178.

[42] E. Cavallari, C. Carrera, T. Boi, S. Aime, F. Reineri, *J. Phys. Chem. B* **2015**, *119*, 10035–10041.

[43] J. Eills, E. Cavallari, C. Carrera, D. Budker, S. Aime, F. Reineri, *J. Am. Chem. Soc.* **2019**, *141*, 20209–20214.

[44] B. Joalland, A. B. Schmidt, M. S. H. Kabir, N. V. Chukanov, K. V. Kovtunov, I. V. Koptyug, J. Hennig, J.-B. Hövener, E. Y. Chekmenev, *Anal. Chem.* **2020**, *92*, 1340–1345.

[45] V. P. Kozinenko, A. S. Kiryutin, A. V. Yurkovskaya, K. L. Ivanov, *J. Magn. Reson.* **2019**, *309*, 106594.

[46] S. Berner, A. B. Schmidt, M. Zimmermann, A. N. Pravdivtsev, S. Glöggler, J. Hennig, D. Von Elverfeldt, J. B. Hövener, *ChemistryOpen* **2019**, *8*, 728–736.

[47] S. Korchak, S. Mamone, S. Glöggler, *ChemistryOpen* **2018**, *7*, 672–676.

[48] See Ref. [41].

[49] J. W. Blanchard, T. Wu, J. Eills, Y. Hu, D. Budker, *J. Magn. Reson.* **2020**, *314*, 106723.

[50] A. AbeIchiro, I. Miura, H. Furuya, *J. Phys. Chem.* **1987**, *91*, 6496–6502.

[51] R. R. Schrock, J. A. Osborn, *J. Am. Chem. Soc.* **1976**, *98*, 2134–2143.

[52] R. R. Schrock, J. A. Osborn, *J. Am. Chem. Soc.* **1976**, *98*, 2143–2147.

[53] "Mechanism of Homogeneous Hydrogenation": F. H. Jardine, *The Metal-Carbon Bond, Vol. 4*, Wiley, New York, **1987**, pp. 1049–1072.

[54] "Homogeneous Hydrogenation of Alkynes and Dienes": A. M. Kluwer, C. J. Elsevier, *The Handbook of Homogeneous Hydrogenation*, Wiley-VCH, Weinheim, **2006**, pp. 374–411.

[55] R. A. Sánchez-Delgado, M. Rosales, *Coord. Chem. Rev.* **2000**, *196*, 249–280.

[56] J. Halpern, D. P. Riley, A. S. C. Chan, J. J. Pluth, *J. Am. Chem. Soc.* **1977**, *99*, 8055–8057.

[57] J. P. Candlin, A. R. Oldham, *Discuss. Faraday Soc.* **1968**, *46*, 60.

[58] R. H. Crabtree, *Homogeneous Catalysis with Metal Phosphine Complexes*, Springer, Heidelberg, **1983**, pp. 297–316.

[59] J. Luo, R. Theron, L. J. Sewell, T. N. Hooper, A. S. Weller, A. G. Oliver, J. S. Mcindoe, *Organometallics* **2015**, *34*, 3021–3028.

[60] P. A. Boeg, J. Ø. Duus, J. H. Ardenkjær-Larsen, M. Karlsson, S. Mossin, *J. Phys. Chem. C* **2019**, *123*, 9949–9956.

[61] D. J. Kennedy, S. J. Seltzer, R. Jiménez-Martínez, H. L. Ring, N. S. Malecek, S. Knappe, E. A. Donley, J. Kitching, V. S. Bajaj, A. Pines, *Sci. Rep.* **2017**, *7*(1), 1–10

[62] K. V. Kovtunov, I. V. Koptyug, M. Fekete, S. B. Duckett, T. Theis, B. Joalland, E. Y. Chekmenev, *Angew. Chem. Int. Ed.* **2020**,

https://doi.org/10.1002/anie.201915306; *Angew. Chem.* **2020**, https://doi.org/10.1002/ange.201915306.

[63] R. W. Adams, J. A. Aguilar, K. D. Atkinson, M. J. Cowley, P. I. P. Elliott, S. B. Duckett, G. G. R. Green, I. G. Khazal, J. Lopez-Serrano, D. C. Williamson, *Science* **2009**, *323*, 1708–1711.

[64] D. A. Barskiy, S. Knecht, A. V. Yurkovskaya, K. L. Ivanov, *Prog. Nucl. Magn. Reson. Spectrosc.* **2019**, *114–115*, 33–70.

[65] S. Knecht, A. N. Pravdivtsev, J.-B. Hövener, A. V. Yurkovskaya, K. L. Ivanov, *RSC Adv.* **2016**, *6*, 24470–24477.